Fluids and Barriers of the CNS

RESEARCH

Open Access

Reduced folate carrier 1 is present in retinal microvessels and crucial for the inner blood retinal barrier integrity

Gokce Gurler[1], Nevin Belder[2], Mustafa Caglar Beker[3], Melike Sever-Bahcekapili[1], Gokhan Uruk[1], Ertugrul Kilic[5,6] and Muge Yemisci[1,4,5*]

Abstract

Background Reduced folate carrier 1 (RFC1; SLC19a1) is the main responsible transporter for the B9 family of vitamins named folates, which are essential for normal tissue growth and development. While folate deficiency resulted in retinal vasculopathy, the expression and the role of RFC1 in blood-retinal barrier (BRB) are not well known.

Methods We used whole mount retinas and trypsin digested microvessel samples of adult mice. To knockdown RFC1, we delivered RFC1-targeted short interfering RNA (RFC1-siRNA) intravitreally; while, to upregulate RFC1 we delivered lentiviral vector overexpressing RFC1. Retinal ischemia was induced 1-h by applying $FeCl_3$ to central retinal artery. We used RT-qPCR and Western blotting to determine RFC1. Endothelium (CD31), pericytes (PDGFR-beta, CD13, NG2), tight-junctions (Occludin, Claudin-5 and ZO-1), main basal membrane protein (Collagen-4), endogenous IgG and RFC1 were determined immunohistochemically.

Results Our analyses on whole mount retinas and trypsin digested microvessel samples of adult mice revealed the presence of RFC1 in the inner BRB and colocalization with endothelial cells and pericytes. Knocking down RFC1 expression via siRNA delivery resulted in the disintegration of tight junction proteins and collagen-4 in twenty-four hours, which was accompanied by significant endogenous IgG extravasation. This indicated the impairment of BRB integrity after an abrupt RFC1 decrease. Furthermore, lentiviral vector-mediated RFC1 overexpression resulted in increased tight junction proteins and collagen-4, confirming the structural role of RFC1 in the inner BRB. Acute retinal ischemia decreased collagen-4 and occludin levels and led to an increase in RFC1. Besides, the pre-ischemic overexpression of RFC1 partially rescued collagen-4 and occludin levels which would be decreased after ischemia.

Conclusion In conclusion, our study clarifies the presence of RFC1 protein in the inner BRB, which has recently been defined as hypoxia–immune-related gene in other tissues and offers a novel perspective of retinal RFC1. Hence, other than being a folate carrier, RFC1 is an acute regulator of the inner BRB in healthy and ischemic retinas.

Keywords RFC1, Blood-retina barrier, Retinal ischemia, siRNA, Lentiviral vector, Trypsin digestion, Pericyte

*Correspondence:
Muge Yemisci
myemisciozkan@gmail.com
Full list of author information is available at the end of the article

Background

The Reduced Folate Carrier 1 (RFC1), also called solute carrier family 19 member 1 (SLC19A1/SLC19a1) is responsible for transporting folates via blood–brain barrier (BBB) to the brain parenchyma [1, 2]. Folates belong to the B9 family of vitamins and are essential for proper functioning of the Central Nervous System (CNS) as they are crucial for many key processes such as histone and DNA methylation, DNA replication and repair, RNA synthesis, methionine production, homocysteine remethylation, amino acid metabolism, neurotransmitter, and phospholipid synthesis [3–6]. Several clinical studies in adults determined that lower serum folate levels could cause neurological dysfunction [7, 8]. Moreover, folate deficiency was shown to result in microvascular complications and increase in oxidative stress in the retina [9–11]. Besides, folic acid reversed vascular tone imbalance of retinal vasculature in individuals with chronic conditions [12]. However, the findings of these studies are chronic consequences that occur with long-term changes and/or deficiency of folates.

Retina is the extension of the CNS, displaying similarities in terms of anatomy, function, and response to insults [13]. The retina has the blood-retina barrier (BRB) that precludes the free transfer of substances from the capillary blood, and is composed of two parts [14]. The outer BRB is constituted of the retinal pigmented epithelium (RPE), which are specialized epithelial cells sealed with tight junctions, residing between the neural retina and a fenestrated capillary network called choriocapillaris. It partly functions to determine the transfer of nutrients from the choriocapillaris to the retina [15]. The inner BRB is established in the inner retinal microvessels and comprises specialized endothelial cells secured by tight junctions, enclosed by basal lamina, pericytes, and perivascular astrocytes; hence it is essential for the maintenance of homeostasis through its selective properties such as harboring specialized nutrient carriers [14]. To date the expression of RFC1 and its transporter function in the retina was primarily evaluated only in the RPE, thus the outer BRB [16–19].

The recent cerebral microvessel transcriptome data showed prominent RFC1 presence in pericytes, the cells crucial with various roles in the regulation of microvascular blood flow and barrier integrity. The retinal microvessels have similar features to the brain [20–22] and are unique for having the highest pericyte ratio in the body. Therefore, our first aim was to investigate the presence of RFC1 protein in the inner BRB, and especially in the pericytes and endothelial cells.

RFC1 has been recently shown in the cell lines to be an importer of immunotransmitter cyclic guanosine monophosphate–adenosine (cGAMP) and other cyclic dinucleotides with robust antitumoral immune response [23] and considered to be the hypoxia–immune-related gene in multiple myeloma patients [24]. The expression and activity of RFC1 was shown to differ during insults like hyperglycemia, nitric oxide exposure, hyperhomocysteinemia and oxidative stress in the RPE [16, 17, 19]. RFC1 polymorphisms in human studies were associated with risk factors for ischemic stroke and silent brain infarcts. However, the role of RFC1 neither in the microvasculature nor in ischemia has been clarified. The retina having similar features to the brain and highest density of pericyte cells makes it an excellent model to investigate the role of the RFC1, shown as one of three common genes in mural cells, and thereby has a potential role in the microcirculation under physiologic conditions or pathological conditions such as ischemia or microcirculatory failure. Therefore, our second aim was to investigate the role of RFC1 protein in the inner BRB in healthy retinas and in acute retinal ischemia which is a worldwide problem for blindness.

In this study, we elucidated the presence of RFC1 protein in the endothelial cells and pericytes of the inner BRB. We employed a custom-designed RFC1-targeted Accell short interfering RNA (siRNA) to silence the RFC1 gene, and a lentiviral vector to overexpress RFC1 in the retinas in vivo. Abrupt and brief changes in RFC1 caused a disruption in the barrier properties of the retinal microvessels. Thus, we identified the immediate role of RFC1 protein in maintaining the inner BRB in health and in acute retinal ischemia.

Methods

Animals

Experiments were performed according to the approval provided by Hacettepe University Animal Experimentations Local Ethics Board (No: 2019/13-06 and 2021/03-19). Adult female and male Swiss albino mice (25–35 g) housed under 12 h of light and 12 h of darkness at standard room temperature (22 ± 2 °C) and 50–60% humidity was used for in vivo experiments. Mice were allowed water and food ad libitum. The recommendations of ARRIVE guidelines and institutional instructions were considered in housing, care, and while performing experiments, the experimental groups were decided in a randomized and blinded manner. For all the surgical procedures intraocular injections, the animals were anesthetized with ketamine (80 mg/kg, intraperitoneal injection, Ketalar®, Pfizer, Cambridge, United Kingdom) and xylazine (8 mg/kg, intraperitoneal injection, Alfazyne® 2%, Alfasan International, Woerden, the Netherlands). A rectal probe connected to the homeothermic blanket with a control unit (Harvard Apparatus, U.S.A.) was utilized to control the body temperature (37.0 ± 0.5 °C).

Pulse rate and oxygen saturation were monitored from the right lower limb via an oximeter (The LifeSense® VET Pulse Oximeter, Nonin Medical Inc., USA). Vital signs (rectal temperature, blood pressure, oxygen saturation, and pulse rate) were kept within physiological limits and recorded. After operations, mice were kept on a homoeothermic blanket until they recovered from anesthesia fully. Next, the mice were kept individually in their cages until sacrificed.

Retinal whole mount preparation

The eyeballs harvested were immersed in 4% paraformaldehyde (PFA) for 1 h, and under a stereomicroscope, we made a puncture at the corneal border with an insulin needle while eyeballs were resting in one drop of Phosphate Buffered Saline (PBS) at room temperature. A circular cut along the limbus was made with the help of a micro-dissector. Following the extraction of the lens and vitreous body, the intact retina was detached from the sclera via a 45° thick curved tip tweezer by going around the edges. Then, the flattened retina was placed into a centrifuge tube consisting of 200 µL PBS for immunohistochemistry.

Retinal radial section preparation

Obtained eyeballs were immersed in 4% PFA for 24 h followed by incubation in 30% sucrose for 2 days. Next, 20 µm sections were obtained by cryostat.

Retinal trypsin digest preparation

We used modified retinal trypsin digestion protocol to isolate retinal microvessels from the surrounding tissue [25]. Retinas were separated in cold PBS, then immersed in 250 µL filtered ddH_20, and, at room temperature, kept on a shaker until they disintegrated. Then kept in 0.3% trypsin (PAN Biotech 1:250) 0.1 M Tris buffer (pH 7.8) in the incubator adjusted to 37 °C. As the separation of microvessels were seen clearly, tissue was washed with dH_2O, and the procedure was repeated until no debris remained. Isolated retinal microvessels were transferred to poly-L-lysine coated slides without disrupting their integrity, and air-dried. This method allowed isolation of the retinal vessels containing endothelial cells, basal lamina, pericytes, the attached perivascular astrocyte processes, without the presence of other cell types like photoreceptor cells.

Immunohistochemical studies

For immunohistochemical studies whole mount retinas, radial sections and isolated retinal microvessels were used. PFA fixed whole mount retinas were kept in in 0.5% PBS-Triton-X, freezed 15 min at − 80 °C and thawed for 15 min at room temperature following overnight incubation in 2% TritonX-100 (Merck Millipore, 1086031000) PBS for permeabilization. They were immersed in 10% normal goat serum for blocking steps for 2 h at room temperature or overnight at + 4 °C. Next, whole mount retinas were incubated at + 4 °C with primary antibodies against RFC1 (SLC19a1, MyBioSource MBS9134642 or Sigma-Aldrich AV44167) for three consecutive overnights. We used two commercial polyclonal antibodies developed against different non-overlapping epitopes of RFC1. RFC1/SLC19a1 antibody from MyBioSource (MBS9134642) was produced against a recombinant fusion protein containing a sequence related to amino acids 452–591 of human SLC19A1 (NP_919231.1), while RFC1/SLC19a1antibody from Sigma-Aldrich (AV44167) was produced against Synthetic peptide directed towards the N terminal region of human SLC19A1 (NP_919231). Then retinas were subsequently incubated with 'Fluorescein' or 'Texas Red' labeled Lectin (Vector Laboratories, Burlingame, CA). Retinal microvessels obtained via retinal trypsin digestion were permeabilized with 0.3% TBS-Triton-X for 30 min, blocked in 10% normal serum of the host of the associated secondary antibody for 1 h at room temperature. Vessel webs were incubated at + 4 °C overnight with primary antibodies against RFC1; for mural cells against PDGFR-β (R&D Systems, AF1042), NG2 (Sigma AB5320A4), CD13 (Acris Antibodies, AM26636AF-N), for endothelial CD31 (BD Bioscience, 550274); for tight junctions ZO-1 (Sigma, MAB1520), Claudin-5 (Invitrogen™, 35-2500), and for Collagen-4 (Abcam, ab6586) (n = 3–6/marker). After several washes, the vessel webs were incubated for 1 h at room temperature with appropriate Cy2-, Cy3- or Cy5-conjugated anti-rabbit IgG (Jackson ImmunoResearch 111-165-144 or 711-175-152) or Cy3-conjugated anti-rat IgG (Thermo Scientific™, A10522, 1:200). To assess the functional inner BRB integrity, PFA fixed whole mount retinas were incubated with Cy3-conjugated anti-mouse IgG (Jackson ImmunoResearch, 115-165-003) at + 4 °C overnight. Later, retinas were incubated with 'Fluorescein' or 'Texas Red' labeled Lectin (Vector Laboratories, Burlingame, CA) at + 4 °C overnight to visualize the vessels. Washed with TBS for 3 times, 5 min each; retinal tissues or retinal microvessels were mounted with a PBS/Glycerol mounting medium consisting of the nuclear staining Hoechst 33258 (Invitrogen™, 1:1000 dilution).

Western blotting

Whole retinas were lysed in Radioimmunoprecipitation assay (RIPA) buffer, sonicated, and homogenized on ice, then centrifuged at 10,000×g at + 4 °C for 20 min. The concentration of the lysates was assessed using BCA protein assay kit (Thermo Scientific™, 23225). After loading

proteins (35 µg/well) to a homemade SDS-PAGE gel, 120 Voltage were applied for 1.5 h. Proteins were then transferred to PVDF membranes by applying 120 mAmp/membrane for 2 h at room temperature. Membranes were incubated with 5% BSA in 0.1% TBS-Tween for 1 h at room temperature for blocking step and incubated with 1:1000 anti-RFC1 antibody produced in rabbit (Sigma-Aldrich; AV44167) at + 4 °C overnight. After washing with 0.1% TBS-Tween, we incubated the membranes with 1:5000 goat anti-rabbit HRP conjugated Invitrogen™, 31460) solution for 2 h at room temperature. For detection, the membranes were treated with a high sensitivity enhanced chemiluminescent (ECL) substrate (Thermo Scientific™, 34096). Imaging was done by Kodak 4000 M Image Station. β-Actin and β-tubulin III (Chemicon, MAB1637) was employed as an internal standard for cell culture homogenates and tissue homogenates respectively. Densitometric measurements were done by ImageJ 1.52 version (NIH, Bethesda, Maryland), and expressed as ratios to the internal standard.

Imaging and analysis

The images of the stained whole mount retinas, retinal microvessels, and retinal radial sections were obtained with Leica TCS SP8 confocal laser scanning microscope (Leica, Wetzlar, Germany) with a diode laser 405, 638 and OPSL 488, 552 nm, with a X, Y, and Z-movement controller, and a high-resolution PMT (Zeiss, Oberkochen, Germany) and HyD (Leica) detectors. Images were either acquired in a single focal plane while keeping settings constant between experimental or control groups for analysis or Z-stack mode with 0.80 µm wide steps along the Z axis. For analysis of immunostained retinal microvessels, 1024 × 1024 pixels and 276.79 × 276.79 µm sized, middle of the Z axis level images was used. Acquired images were exported as 8-bit grayscale.tiff formats from Leica Application Suite X (LAS X; version 3.5.5.19976) and opened in ImageJ 1.52 version. First, the lectin frame of each image was filtered by Gaussian blur (sigma = 4) to reduce the random noise, and Huang Thresholding was applied to mask the lectin-positive microvessel areas of the images. After de-speckling (Process tab > Noise > Despeckle) and eroding (Process tab > Binary > Erode), the binary image was divided by 255 using Math function (Process tab > Math > Divide) to convert microvessel pixels to "1" and background pixels to "0". Later, either "RAW" lectin image or the overlapping grayscale image belonging to tight junctions or collagen-4 was divided by the binary of the lectin image. This created 32-bit grayscale images in which microvessels had singular intensity and the background had infinity. Finally, the mean grey value (RFU, range between 0 and 255) was obtained which corresponded to the mean intensity of the pixels occupying the microvessel area. Number of pericytes were quantified from Lectin and Hoechst labelled microvessel preparations by researchers blinded to the experimental or control groups. As pericytes are well known to have protruding nuclei, they were easy to distinguish morphologically and spatially from endothelial cells having flat nuclei. The total microvessel length was measured with AngioTool (v 0.6a (64 bits), October 2014) software, and pericyte number per millimeter (mm) of microvessel length was calculated [26]. IgG extravasation was calculated from the 150 × 150 µm sized ROIs of 8-bit grayscale.tiff format images of wholemount retinas labeled with Cy3-conjugated anti-mouse IgG and lectin. The IgG and lectin frames were applied Huang Thresholding to detect the IgG and lectin-positive pixel counts. After thresholding, the binary images were divided by 255 to convert IgG positive and lectin positive pixels to "1" and background pixels to "0". Next, the IgG positive pixel counts are divided into lectin positive pixel counts.

To further explore localization of RFC1, we performed double immunostainings with endothelial marker CD31 which is distributed over the entire endothelial cell surface, luminal, abluminal, and lateral [27] allowing us to label the whole endothelial cell surface. We employed radial cryo-sections of retinas from PFA fixated eyeballs which allows us to visualize the luminal surface of retinal microvessels. We also performed immunostainings with two types of antibodies which were targeted to two different regions of RFC1 protein to eliminate the possibility of antibody-related variations in distribution. Imaging was performed on confocal laser scanning microscope (Zeiss LSM 980 with Airyscan 2) with 40 × magnification (W-Plan Apochromat 40x/1.0 DIC VIS-IR M27) that allowed us to perform super-resolution confocal imaging with Airyscan detector technology.

To measure the potential microvessel diameter changes in retinal microvessels, images from lectin-labelled retinal trypsin digest preparations were used. Pericyte-associated vascular diameter of individual pericytes per microvessel branch was measured as described before. Briefly, to account for changes in pericyte position relative to the vessel wall, the measurements were taken at juxtanuclear sections perpendicular to the vessel axis. The mean of each juxtanuclear section per pericyte was calculated and divided by the initial diameter of each vascular segment to provide an intrinsic baseline correction. This resulting value was defined as the "juxtanuclear diameter ratio" [28].

To structurally assess retinas, we labeled radial cryo-sections of 20-µm thick retinas from PFA fixated eyeballs with β-Tubulin III (as a ganglion cell marker), lectin and Hoechst 33258. To standardize,

four individual sections that included optic nerve were chosen and ROI were determined from either side of the optic nerve in every section. We determined the number of ganglion cells (GC number), total thickness of retinal sections, inner nuclear layer thickness (INL thickness; which predominantly includes bipolar cells), and outer nuclear layer thickness (ONL thickness; which predominantly includes photoreceptors) in retinal sections. To evaluate GC survival, the number of β -Tubulin III positive, lectin negative cells were counted manually in four sections in ROIs which were placed to cover 250 µm retinal section length (Additional file 2: Fig. S2F).

Gene silencing in vivo by short interfering RNA (siRNA)

To silence RFC1 gene, we used two custom-designed mouse RFC1 (Slc19a1) Accell siRNAs targeted to two different regions of RFC1 mRNA and two Accell scrambled (control) siRNAs (Horizon Discovery, Waterbeach, United Kingdom). Accell siRNA has several advantages as it does not need any transfection reagents which may have unwanted effects when applied in vivo. Furthermore, they could be internalized by any type of mammalian cells [29]. Accell siRNAs have been previously proven to be uniformly distributed across rat retinal tissue and successfully inhibit various genes following intravitreal delivery [30]. Product codes of siRNAs with sequences are given in Table 1. RFC1-siRNA-1 and RFC1-siRNA-2 or scrambled (control) siRNA-1 and 2 were pooled in equal volumes for administration to improve the potency and specificity.

We delivered 100 µM pooled RFC1-siRNAs or Control-siRNAs intravitreally to the eyes (2.3 µL/ eye) of animals via 33 G Neuros Syringe (1701 RN, Hamilton). We did not utilize contralateral eyes as controls to avoid the possible transfer of siRNAs to the opposite side [31, 32]. After 24 h, we either proceeded to retinal ischemia or sacrificed mice, and determined the levels of mRNA or protein.

Table 1 The product codes and the sequences of sense strands of RFC1-siRNAs and scrambled (control) siRNAs

	Product codes	Sequences of sense strand
RFC1-siRNA-1	A-044248-13	C.C.A.G.C.C.U.A.C.U.U.C.A.U.G.C.U.U.U.U.U
RFC1-siRNA-2	A-044248-15	C.C.A.G.G.A.A.A.C.U.A.G.A.U.C.G.C.A.U.U.U
Scrambled siRNA-1	D-001910-01	U.G.G.U.U.U.A.C.A.U.G.U.C.G.A.C.U.A.A.U.U
Scrambled siRNA-2	D-001910-03	U.G.G.U.U.U.A.C.A.U.G.U.U.U.U.C.C.U.A.U.U

Gene overexpression in vivo by lentiviral vector (LV)

Lentiviral vectors (LV) that express either green fluorescent protein (GFP) (Control-LV) or GFP with RFC1 (RFC1-LV) driven by EF-1 alpha promoter were used to overexpress RFC1 gene in the retina.

The lentiviral packaging system used for RFC1-LV or Control-LV was second-generation and was an effective and safe technique in production. Total RNA from cultured mouse neuro 2a cells was extracted using AllPrep DNA/RNA/Protein Mini Kit (80004, Qiagen, Hilden, Germany) following the manufacturer's instructions. Transcriptor First Strand cDNA Synthesis Kit (04896866001, Roche, Basel, Switzerland) was used to obtain complementary DNA (cDNA). The coding region of Mus musculus SLC19a1 variant 1/RFC1 (NCBI Reference Sequence: NM_031196.3) was amplified with specific primers (forward 5′-agtcagaattcatggtgcccactggccag-3′and reverse 5′-AGT CAGGATCCTCAAGCCTTGGCTTCGACTCTT -3′) with fast digest restriction enzymes EcoRl (FD0274, Thermo Fisher Scientific, Massachusetts, USA) and BamHI (FD0054, Thermo Fisher Scientific). Restriction enzymes BamHI and EcoRI were used to digest the PCR product of SLC19a1 and expression plasmids (pLenti-EF1α-GFP-2A-Puro; Applied Biological Materials, Richmond, Canada). Subsequently, ligation was realized with T4 DNA ligase (EL0014, Thermo Fisher Scientific). Sequencing pMD2.G and psPAX plasmids, kindly provided by Dr. Didier Trono (Ecole Polytechnique Federale, Lausanne, Switzerland), were used to confirm the insert. They were employed as complementary vectors of the packaging of the lentiviral system (12259; 12260, Addgene, United Kingdom). HEK293T cell line (6×10^6 cells) was chosen to be seeded on 10 cm plates (CLS3294, Corning, New York, USA). The following day, the vector transfection Lipofectamine 3000 (L3000015, Thermo Fisher Scientific) was applied according to the manufacturer's instructions. Shortly, 7 µg lentiviral vector, 3.5 µg pMD2.G, and 7 µg psPAX were used to prepare DNA-lipid complexes. The DNA-lipid complex was added slowly after 10 min of incubation at room temperature. Six hours after transfection, the medium was changed with fresh DMEM (P04–01158, Pan Biotech, Bavaria Germany) and was incubated at 37 °C in a humid atmosphere consisting of 5% CO_2. Twenty-four and fifty-two hours following the transfection, the medium was harvested, centrifuged (10 min at 2000 rpm), and filtered with a low binding filter with a 0.45 µm pore size. After ultra-centrifuging (120,000 g for 2 h), viral particles were dissolved

in Dulbecco's Phosphate Buffered Saline (DPBS) without calcium and magnesium (P04–3650, Pan Biotech). The plasmid with no DNA inserted was packaged with the same procedures to use as a control. The viral titer (1×10^8 lentivirus particles in 1 µl 0.1 M PBS) was measured by a previously published protocol [33].

LV (1×10^8 lentivirus particles in 1 µl 0.1 M PBS) were intravitreally delivered to the retina (2 µL/eye) via 33 G Neuros Syringe (1701 RN, Hamilton).10 days after the delivery, we either proceeded to retinal ischemia or sacrificed mice to obtain eyeballs.

Quantitative reverse transcriptase-polymerase chain reaction (qRT-PCR)

Eyeballs were freshly dissected in ice-cold sterile PBS under a surgical microscope to get the retina intact. The RNA from whole retinas was extracted via TRIzol Reagent (Invitrogen) according to the manufacturer's guidelines. The retinal RNA was then reverse transcribed to cDNA with a high-capacity reverse transcription cDNA kit (Applied Biosystems). Primer pairs specific to mouse RFC1/SLC19a1 (Mm00446220_m1) and Tubb4a (Mm00726185_s1, beta 4A class IVA as a housekeeping gene) were constructed and verified by Life Technologies to use with TaqMan qPCR chemistry (TaqMan™ Gene Expression Assay, Applied Biosystems™, 4331182). Amplicon context sequences for SLC19a1 and beta 4A class IVA are shown in Table 2. qRT-PCR analysis was performed to calculate the relative fold change in mRNA expression level of the SLC19a1 after siRNA administration. The critical threshold cycle (CT) of SLC19a1 gene was first normalized to the beta-tubulin 4A with the comparative CT method. The ΔCT which is the difference in CT values between the SLC19a1 and beta-tubulin 4A genes were then normalized to the corresponding ΔCT of the control siRNA group, expressed as ΔΔCT and calculated as fold change ($2-^{\Delta\Delta CT}$).

Electroretinography (ERG)

A modified scotopic ERG protocol [34] was performed on mice that were kept in complete darkness for 24 h before ERG. Anesthetized mice were placed on a heating pad in prone position. To record the electrical activity in the eye, three electrodes were used. The ground electrode was a needle electrode was inserted beneath the skin at the base of the tail, the reference electrode was inserted in the mouth, and the measuring electrode was placed in contact with the cornea of the eye being measured. Pupils were dilated with topical administration of 2.5% phenylephrine. The eyeballs were protruded by tightening a loop of a simple knot that was circumferentially slipped over the eyeball. After moistening the cornea with saline (0.9% NaCl), the eye was presented with blue LED flashes in 5 V potential, with repeat rate 0.2 Hz and pulse width 0.01 s. The band pass filters were set to 1–1000 Hz. The signals were recorded and analyzed by PowerLab 16/35 data acquisition system and displayed by LabChart Reader 8 (AD Instruments).

Retinal ischemia model

The retinal ischemia model used here was previously developed in our laboratory [35]. In brief, anesthetized mice were put in a prone position under a stereoscope (SMZ1000, Nikon Instruments Inc., Amsterdam, The Netherlands) and their heads were immobilized with a nosepiece. Central retinal arteries located in the central optic nerve were exposed via cautious retroorbital dissection. A small strip (0.3×1 mm) of 30% $FeCl_3$—soaked filter paper was placed on the optic nerve for 3 min to trigger clot formation and occlude the central retinal artery. Based on our previous observations, we used 1 h of ischemia, as it was sufficient to induce ischemic changes in the microcirculation such as mural cell contractions [20, 21]. One hour later, eyeballs were

Table 2 Gene symbols the full names of the genes, accession number of transcripts and amplicon context sequences of SLC19a1 and beta 4A class IVA

Symbols	The full names of genes	Accession numbers of transcripts	Amplicon context sequences
RFC1/SLC19a1	Mus musculus solute carrier family 19 (folate transporter), member 1 [Mus musculus (house mouse)]	NM_031196.3:1240–1390	CGGGACATCTGGGTGTGCTACGTGACCTTTGTG CTTTTCCGTGGGGCCTACCAGTTCCTTGTGCCC ATTGCCACTTTTCAGATTGCGTCTTCCCTGTCTAAA GAGCTCTGTGCATTGGTCTTTGGGATCAACACT TTCCTAGCTACTGCGC
Tubb4a	Mus musculus tubulin, beta 4A class IVA (Tubb4a)	NM_009451.3:1852–2030	CCACCTTCTTAGATCTTGAAAATCCTTTCCTTTATG CCCTGTCCCTTCCCCAGCACTCCTGAACCATTC TCCTCCACCTCTGACATGCCCAGATATTTCTCTAGA TCTTAACATTTTCCCCAGCCTCCAAGTCCTCTC ACCTTGCCTTACCTCTGACCTCACAGCTACCCA CTCCTGAC

collected under anesthesia, and animals were sacrificed by cervical dislocation.

Statistical analyses

All in vivo experiments were repeated in at least n = 3 mice/group. The number of mice per group for in vivo experiments are mentioned in the figure legends. All results were conveyed as mean ± standard error of the mean (S.E.M.). Data were analyzed using IBM SPSS 23. Non-normally distributed data were compared using the Mann–Whitney U test (for two groups). The expression ratio in a treatment group was expressed as a percentage of the ratio in the control group. $p \leq 0.05$ was considered significant.

Results

RFC1 protein is abundantly expressed in the endothelial cells and pericytes of the inner BRB

The scarcity of antibodies for RFC1 immunohistochemistry [23] until recently was a challenge for studies; hence, most former studies used RFC1 antiserum or homemade antibodies to mark RFC1 protein in the tissues [23, 36, 37]. The availability of commercial RFC1 antibodies that were confirmed by immunohistochemistry and by Western Blotting [1, 2] facilitated the research in the field.

We first immunohistochemically examined RFC1 in the radial retina sections, and as expected, determined that RPE was immunopositive (Fig. 1A). This was also confirmed in whole mount retina preparations (Fig. 1B) [38]. RFC1 immunopositivity was also found in the

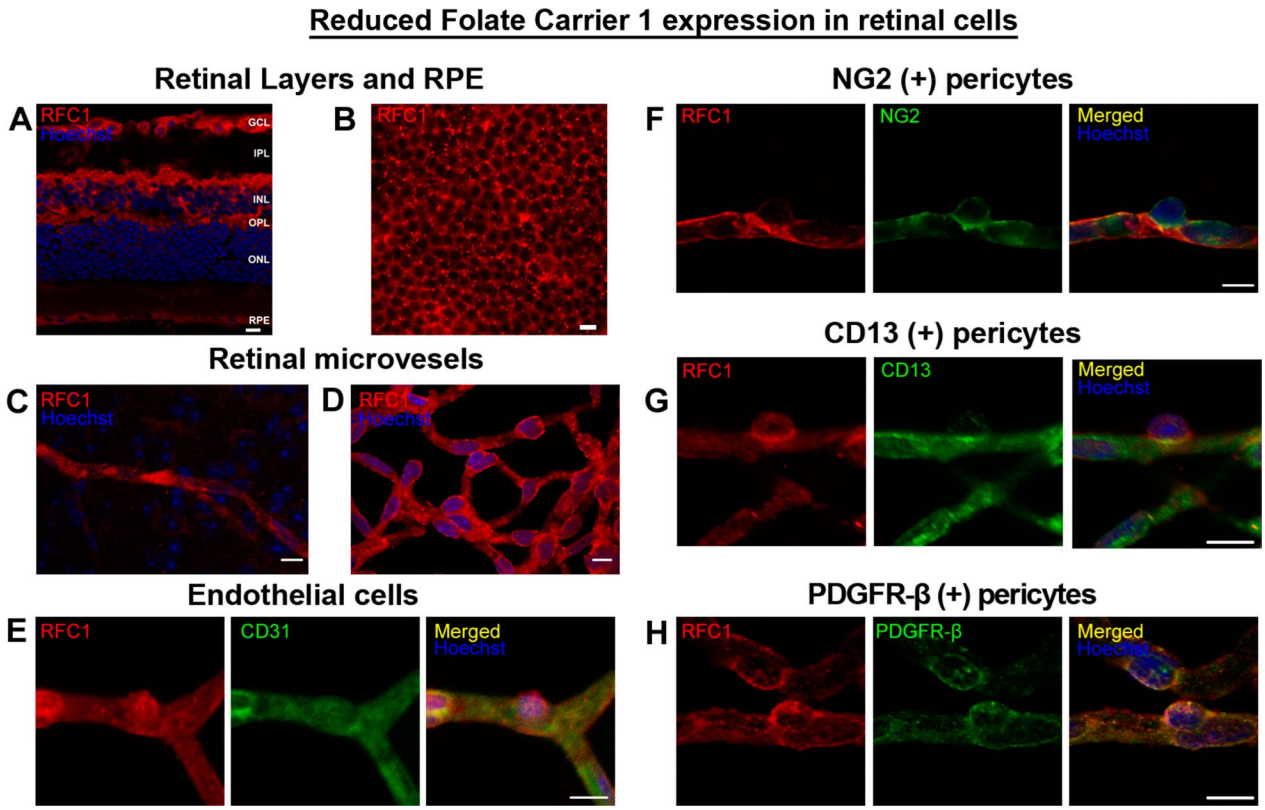

Fig. 1 RFC1 protein is abundantly expressed in endothelial cells and pericytes of the retinal microvessels. **A** Ex-vivo labeling of 20 µm radial cryo-section from PFA fixated eyeballs of naive Swiss Albino mice with anti-RFC1 antibody (red). Abundant RFC1 immunopositivity is observed along ganglion cell layer (GCL), inner plexiform layer (IPL), outer plexiform layer (OPL) where retinal microvessels forms vascular horizontal vascular beds; as well as the retinal pigment epithelium (RPE). However, this preparation limited the observation of microvessels, hence inner BRB, as it commonly included microvessels circularly rather than longitudinally. Scale bar= 25 µm **B** RPE which is known to express RFC1 previously is well stained with anti-RFC1 antibody (red) as our positive control. **C** The microvessels constituting inner BRB form the deep vascular plexus of the retina were immunohistochemically labelled with anti-RFC1 antibody in PFA fixated whole-mount retinas. **D** Retinal microvessels which were obtained via retinal trypsin digestion method that allowed to get only microvessels (< 9 µm diameter) were immunofluorescently labeled with anti-RFC1 antibody (n = 6 retina; red). Nuclei were labeled with Hoechst 33258 (blue) in all the rows. **E** The endothelial marker CD31 (green) (n = 3). The "bump-on-a log" shaped pericyte body was positively stained with anti-RFC1 antibody, but negative for endothelial marker CD31. Hence, RFC1 staining was specific. **F**–**H** RFC1 (red) also colocalized with accepted pericyte markers NG2, CD13, PDGFR-β (green) shown respectively (n = 3/marker). Nuclei were labeled with Hoechst 33258 (blue). Scale bars = 10 µm

ganglion cell layer (GCL), inner and outer plexiform layers (IPL and OPL) that coincided with the superficial and deep microvascular plexus. Hence, the RFC1 immunosignal was identified in the retinal layers comprising microvessels (Fig. 1A, C). We used two different antibodies, high concentrations, and long incubation durations like three overnights at + 4 °C with the primary antibody for the 200 µm thick whole mount retinal preparations to visualize retinal microvessels. Likewise, isolating retinal microvessels with the trypsin digestion method provided us with an easier and more consistent preparation for immunostainings.

We observed that RFC1 was distributed continuously and diffusely throughout the retinal microvessels (Fig. 1D). RFC1 was immunohistochemically co-labeled with the endothelial marker, CD31, whose immunoreactivity exclusively outlined the endothelial cells. As a convincing finding that there was no crosstalk in immunoreactivity, RFC1 labeling was determined to colocalize with both the endothelial cells, and the 'bump on a log' shaped cells (Fig. 1E), which designates pericytes.

We then labeled the microvessels with well-defined pericyte markers including the neural/glial antigen 2 (NG2), aminopeptidase-N (CD13), and platelet-derived growth factor receptor beta (PDGFR-β) all of which showed colocalization with RFC1 (Fig. 1F–H). These indicated that RFC1 protein was present both in the endothelial cells and pericytes. Additionally, we performed double immunostainings with endothelial marker CD31 distributed over the entire endothelial cell surface, luminal, abluminal, and lateral [27]. This allowed us to label the whole endothelial cell surface on radial cryosections of retinas and to visualize the luminal surface of retinal microvessels. Our immunostainings have resulted in both luminal and abluminal labeling (Additional file 1: Fig. S1).

Retinal RFC1 is downregulated in vivo by RFC1 targeted Accell siRNA, and leads to disruption of the inner BRB

We delivered a combination containing the same amount of specifically designed two RFC1 targeted Accell siRNAs (RFC1-siRNA) or two scrambled siRNAs intravitreally and sacrificed the mice 24 h later. To confirm the knockdown of RFC1, we obtained fresh whole retinas and determined a pronounced decrease in RFC1 protein via Western Blotting ($p = 0.028$; Fig. 2A, B). Additionally, RFC1-siRNA significantly decreased RFC1 mRNA by 24.75% compared to scrambled siRNA ($p = 0.004$, Fig. 2C). In line with these, RFC1 immunosignal intensity was diminished in the microvessels of RFC1-siRNA injected retinas when mean grey value of RFC1 immunosignal (i.e., fluorescence intensity) was measured (72.1%, $p < 0.0001$; Fig. 2C, D). We also noticed that RFC1-siRNA treated retinas were fragile, and prone to damage during the procedures.

The immunostaining of the whole mount retinas also confirmed RFC1-siRNA knockdown with diminished RFC1 immunosignal, and further showed that Lectin staining was weaker and interrupted in RFC1-siRNA treated preparations, indicating that microvessels might be structurally damaged (Fig. 2H). In addition, these retinal microvessels demonstrated lower NG2 signal compared to scrambled-siRNA treated ones, which suggested that pericytes might also be damaged by RFC1-siRNA (Fig. 2E). However, to address if the reduction in RFC1 immunoreactivity in siRNA treated microvessels might be associated with the change in microvascular tonus, we assessed the pericyte-associated vascular diameter in each microvessel branch. We found no change in juxtanuclear diameter ratio between RFC1-siRNA and scrambled-siRNA treated groups (Fig. 2F). Next, we assessed the loss of pericytes, we assessed pericyte density (soma per mm capillary). We found no significant decline in

(See figure on next page.)

Fig. 2 The validation of Accell siRNA mediated in vivo RFC1 knockdown, which led to a reduction in critical proteins of the inner BRB. **A** Western blotting image of retinas (n = 4 mice/group) depicting the robust decrease in RFC1 protein of RFC1-siRNA delivered ones compared to scrambled-siRNA. β-Tubulin III was loading control. 35 µg protein was loaded for each retina. **B** The graph illustrates the quantification of the relative band densities of given Western blotting image which expresses RFC1 band density in proportion to β-Tubulin III, which shows decrease in relative protein levels in RFC1-siRNA treated retinas (*p = 0.028). **C** The graph shows that RFC1-siRNA delivery reduced retinal RFC1 mRNA levels by 24.75% when compared to scrambled-siRNA (*p = 0.004). **D** The graph illustrates the percentage of mean grey value of RFC1 frame in lectin positive microvessel area in RFC1-siRNA treated group normalized to scrambled-siRNA treated group as described in Methods section. RFC1-siRNA delivery significantly reduced the percent of the mean grey values of RFC1 by 72.10% (n = 4). Representative confocal images of Scrambled-siRNA or RFC1-siRNA delivered retinal microvessels stained by anti-RFC1 antibody (red). **E** RFC1-siRNA treated retinal microvessels showed less NG2 immunosignal compared to scrambled-siRNA treated ones, indicating that pericytes might also be damaged by RFC1-siRNA. **F** However, juxtanuclear diameter ratio of total of 97 pericyte-associated microvessels were measured (n=3/group) and no significant changes were found. The dots represent the mean of each juxtanuclear section per pericyte and divided by the initial diameter of each vascular segment. **G** Also, pericyte body counts per microvessel length (mm) were not different between the groups, n = 3 images were analyzed per animal. **H** Whole mount retinas were labeled by anti-RFC1 antibody (red) and Fluorescein lectin (green). RFC1 immunosignal was decreased and interrupted along deep retinal microvessels. Also, lectin signal was weakened in RFC1-siRNA treated retinas representing the structural decomposition of microvessels. **I-L** RFC1-siRNA delivery significantly reduced the percent of the mean grey values of collagen-4 68% (n=4), occludin 57.03% (n=3), claudin-5 76.26% (n=4), and ZO-1 53.22% (n=4). The reductions that are statistically significant represented as *$p \leq 0.05$. Nuclei are labelled with Hoechst 33258 (blue), Data are mean ± S.E.M, Mann–Whitney U; Scale bars= 10 µm

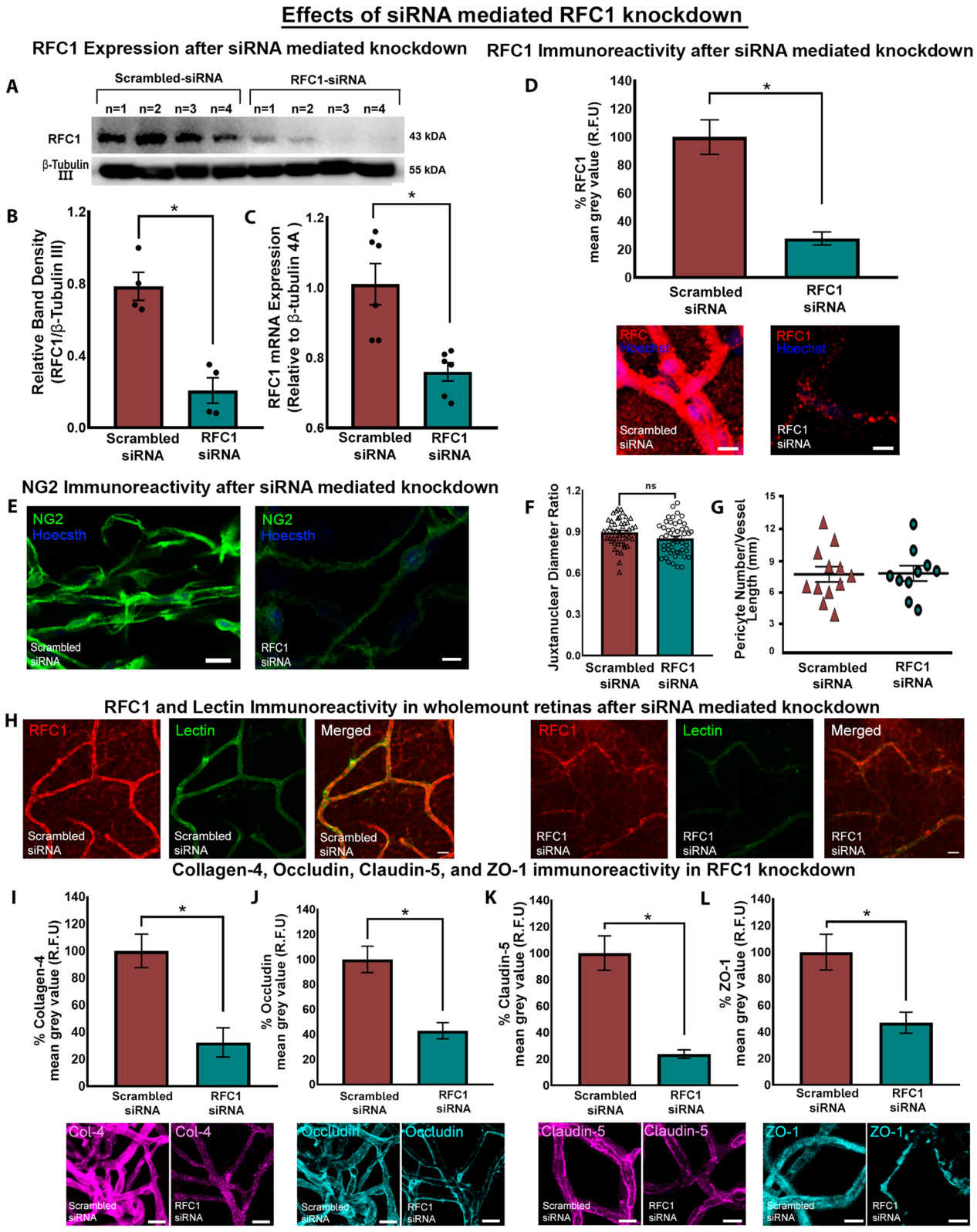

Fig. 2 (See legend on previous page.)

pericyte density in RFC1-siRNA administered retinas suggesting that RFC1 decrease may not affect pericyte maintenance, as it did not reduce pericytes in number at least at this time point (Fig. 2G). However, we could not exclude disruption of pericyte functions via RFC1-siRNA since there is marked decline in the expression of pericyte marker NG2.

As we determined that retinal microvessels express RFC1 protein abundantly, and we could efficiently knock down RFC1 in vivo, we elucidated whether RFC1 suppression may lead to any changes in the inner BRB.

Strikingly, knocking down retinal RFC1 diminished immunoreactivity of the tight junction-associated transmembrane proteins occludin, claudin-5, and cytoplasmic adaptor protein zonula occludens-1 (ZO-1), as well as the main basement membrane protein collagen-4 in trypsin digested microvessels (Fig. 2H–K). In RFC1-siRNA treated microvessels, immunoreactivity of collagen-4 that surrounds the abluminal membrane of endothelial cells and covers pericytes residing in the basement membrane decreased by 68% ($p=0.0043$), occludin decreased by 57.03% ($p=0.0043$), and claudin-5 decreased by 76.26% ($p=0.0006$). ZO-1, the intracellular adaptor protein establishing a link between occludin and intracellular actin cytoskeleton decreased by 53.22% ($p=0.0012$).

Moreover, the changes observed in the inner BRB were not associated with immersive structural damage. In morphological analysis of retinal radial sections, we observed no significant difference in GC number, total retinal, INL and ONL thickness between control and RFC1-siRNA group indicating RFC1-knockdown did not lead to an overall structural and morphological damage (Additional file 2: Fig. S2F). Furthermore, the ERG showed that the scotopic a- and b-wave amplitudes of RFC1-siRNA and scrambled-siRNA treated retinas were similar suggesting no worsening of the rod photoreceptor and the inner retina functions (Additional file 2: Fig. S2A, B, C). The implicit time a-wave peak remained unaltered between our experimental and control groups (Additional file 2: Fig. S2D). However, interestingly, the implicit time b-wave peak increased in RFC1-siRNA treated retinas (Additional file 2: Fig. S2E, $p=0.029$), which suggests that there was a delay in the speed of the signal transmission through the bipolar cells in the retina.

Retinal RFC1 is upregulated in vivo by LV overexpressing RFC1, and this upregulation changes the inner BRB properties

Next, we aimed to increase the expression of RFC1 in mouse retinas via LV carrying RFC1 as described in detail in the methods section. We preferred the LV gene delivery method due to its efficiency to induce stable gene expression, its tropism to the inner retina and the cells of retinal microvessels when delivered intravitreally [39, 40].

The efficient RFC1 protein overexpression was shown by Western Blotting in cell lysates (Fig. 3A). Subsequently, we proceeded to validate the in vivo LV-mediated transduction. Mice had unilateral intravitreal LV injections. No animals developed any local infections. The eyeballs of mice ($n=3$) that received intravitreal Control-LV bearing GFP were harvested ten days after. The retinal and perimicrovascular cells showed GFP expression disclosing that the cells were infected with LV (Fig. 3B).

The overexpression of RFC1 by LV in the retina was also observed immunohistochemically. RFC1 immunoreactivity revealed a marked intensity increase in both the retinal whole mount and retinal microvessel preparations in RFC1-LV compared to Control-LV (Fig. 3C, D) with 167.5% increase in RFC1 immunosignal ($p=0.0159$; Fig. 3D).

As the suppression of RFC1 levels led to an extensive structural damage in retinal microvessels, we further investigated whether RFC1 overexpression had any effects. Immunohistochemistry of tight junction proteins (occludin, claudin-5), intracellular adaptor protein ZO-1, and main basement membrane protein collagen-4 in retinal microvessels (from $n=3$ retina/per marker, Fig. 3E–H) were done 10 days after administration. RFC1-LV administered retinal microvessels displayed increased immunosignal in occludin ($p=0.0059$), claudin-5 ($p=0.0040$), and collagen-4 ($p=0.0159$) compared to Control-LV ones (Fig. 3E–G). However, the immunosignal of ZO-1 did not differ between the groups (Fig. 3H).

Retinal ischemia alters RFC1 protein and decreases the inner BRB proteins which can be ameliorated by RFC1 overexpression

After observing the potential role of RFC1 protein in maintaining the inner BRB, we investigated whether RFC1 protein has a role in retinal ischemia. We made 1 h permanent retinal ischemia, as it is considered sufficient to observe microvessel-related changes such as capillary constrictions or protrusion of the contracted pericyte soma from the microvessel wall (Fig. 4C, asterisk), and yet an early time point to allow us to minimize the effects of inflammation [20–22].

Following ischemia, the expression of RFC1 protein was enhanced significantly compared to controls detected by Western blotting ($p=0.025$; Fig. 4A, B) and RFC1 immunopositivity ($p<0.0001$; Fig. 4C). The pronounced RFC1 signal was detected in the protruding pericytes (Fig. 4C, white arrows) probable of an increased signal in affected cells.

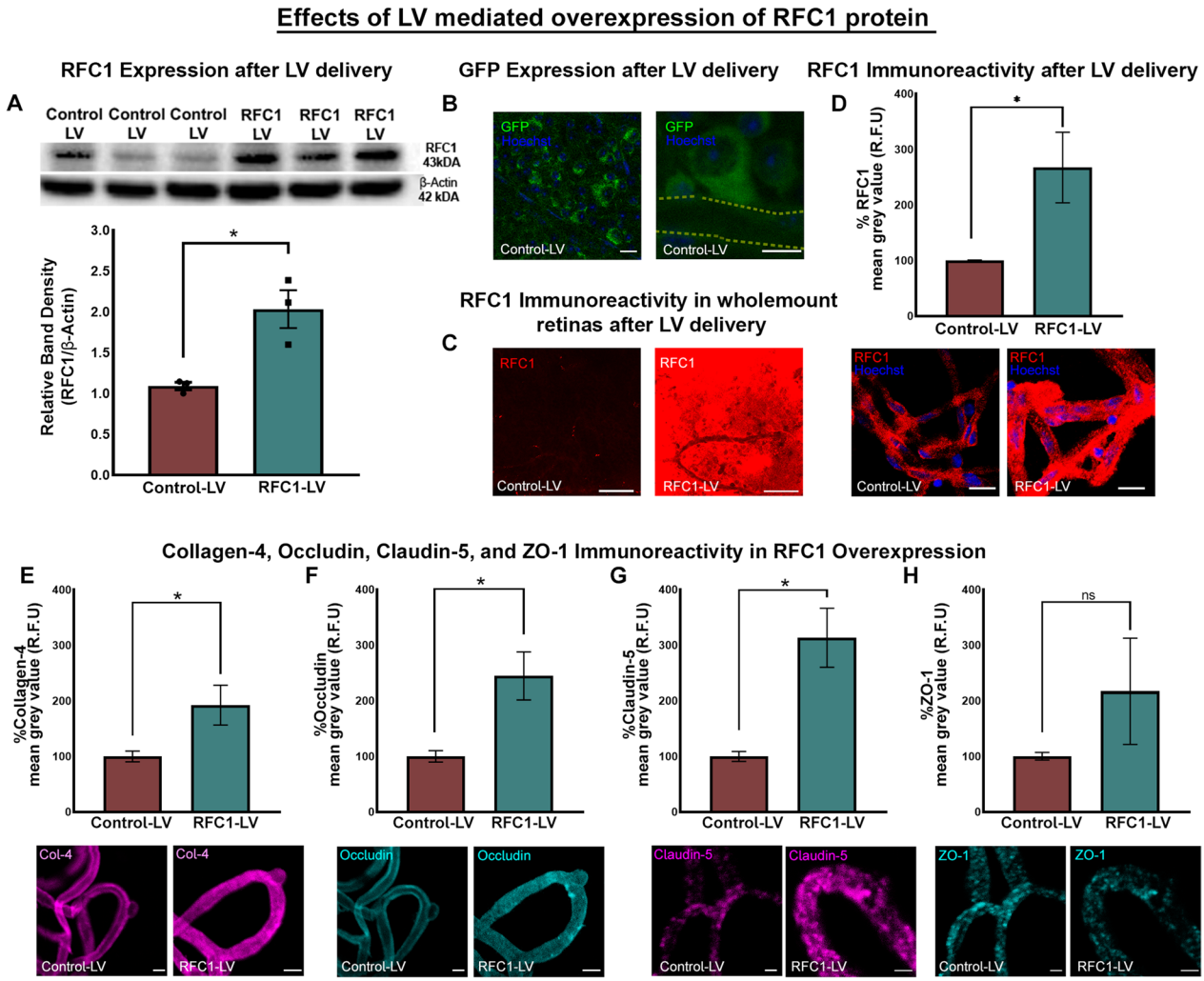

Fig. 3 The validation of lentiviral vector-mediated overexpression of RFC1 protein in vivo, which led to an increase in the proteins of BRB. **A** The Western Blotting image shows corresponding overexpression of RFC1 protein in RFC1-LV transduced neuroblastoma cells (N2a) compared to Control-LV transduced cells. For cell culture lysates, Beta-Actin was the loading control. The graph illustrates the quantification of the relative band densities of given Western blotting image which expresses RFC1 band density in proportion to β-Actin, which shows increase in relative protein levels in RFC1-LV treated retinas (*p = 0.016). **B** The confocal images from whole mount retinas confirmed the intravitreal delivery of Control-LV into the mouse eye showing lentiviral vectors infected various retinal cells, as reporter gene GFP (green) signal indicated. Also, as magnified image showed, perivascular cells and pericytes expressed GFP protein in LV-RFC1 or Control-LV injected retinas, microvessel trace was shown by dashed line. **C** The representative images of whole mount retinas which had been treated by LV-RFC1 showed increased RFC1 immunosignal (red) compared to Control-LV injected control retinas (n = 3). **D** The graph illustrates the percentage of mean grey value of RFC1 frame in lectin positive microvessel area in RFC1-LV treated group normalized to Control-LV treated group as described in Methods section. RFC1-LV delivery significantly increased the percent of the mean grey values of RFC1 (n = 3). **E**–**H** RFC1-LV delivery significantly increased the percent of the mean grey values of collagen-4 (n = 4), occludin (n = 3), claudin-5 (n = 3), but not ZO-1 compared to Control-LV delivered groups. (*p ≤ 0.05). Collagen-4 (magenta), occludin (cyan) lectin (Yellow) immunosignal increased as well as claudin-5 (magenta) except ZO-1 (cyan) via RFC1-LV treatment compared to Control-LV treatment. Nuclei were labelled with Hoechst 33258 (blue) Data are mean ± S.E.M. Mann-Whitney U; Scale bars= 10 μm

We studied whether retinal ischemia caused any alterations in the inner BRB proteins and observed that 1 h retinal ischemia decreased collagen-4 and occludin immunosignal compared to controls (p = 0.0140, p = 0.0317 respectively; Fig. 4D, E). In addition, pretreatment with LV-RFC1, 10 days before ischemia led to increase in collagen-4 and occludin immunosignal compared to Control-LV delivered ones indicating that overexpression of RFC1 before ischemia might reverse the loss of ischemia-induced collagen-4 and occludin (p<0.0001, p = 0.039 respectively; Fig. 4 F, G).

Finally, we studied whether RFC1-siRNA knockdown induced disruption of the inner BRB proteins resulted in barrier dysfunction. We stained vessels with lectin

and determined endogenous IgG extravasation by fluorescently labeled anti-mouse IgG antibody (Fig. 5A, red arrows). RFC1-siRNA treated mice displayed endogenous IgG leakage (Fig. 5A, red arrows), while scrambled-siRNA treated retinas did not show any. This indicated that RFC1 is essentially required for the structural and functional integrity of the inner BRB in health.

On the other hand, we observed no IgG extravasation after 1 h retinal ischemia, so it significantly did not compromise the integrity of inner BRB (Fig. 5B). This observation was consistent with the literature since 1 h retinal ischemia causes early changes such as capillary constrictions (white arrows, Fig. 5B), but it does not suffice for the inner BRB disruption to the extent of allowing endogenous IgG (150 kDa) leakage through paracellular barrier even if disintegration of tight junctions commenced [41–43]. We then studied whether knocking-down RFC1 before ischemia may provoke disruption of the inner BRB. When RFC1-siRNA was administered 24 h before retinal ischemia, a significant amount of endogenous IgG extravasation was determined (Fig. 5B, red arrows). As scrambled-siRNA administration 24 h before retinal ischemia led to no apparent IgG extravasation, this indicated that decreased RFC1 levels accelerated the inner BRB disruption in acute retinal ischemia.

Discussion

In this study, we demonstrated the presence of RFC1 protein in the endothelial cells and pericytes of the inner BRB of mice. We also showed that RFC1 is an essential component for maintaining the inner BRB and has fundamental roles in retinal ischemia.

RFC1 expression at the protein level in the endothelial cells and pericytes of retina has never been studied before, despite its consistent detection in the transcripts of mural cells (pericytes and vascular smooth muscle cells) of the brain [44]. A previous in vitro study examined the transport kinetics of folate in rat inner BRB model and identified RFC1 as the primary responsible transporter for folate by examining RFC1 at the mRNA level [45]. Besides, a recent study characterized the localization of folate transporters, hence RFC1 expression at CNS barriers in detail focusing especially on BBB cells including the endothelial cells; however, this study explored neither the retina nor pericytes [46]. So, our study offers a recognition for the roles of RFC1 protein in the CNS and deepens our understanding of other critical functions as well as novel treatment strategies for brain disorders.

Isolating retinal microvessels with the trypsin digestion method provided us an easier and consistent preparation for immunostainings. Our results highlight that, retinal endothelial cells, like their counterparts in the CNS, express RFC1 protein. As an additional novel finding we detected the colocalization of RFC1 with the well-defined pericyte markers. Most studies evaluating the role of RFC1 in microvessels concentrated on only the endothelial cells, but not the neighboring pericytes [1, 2, 36, 47]. Our findings actually match the results of a recent meta-analysis combining five different mouse brain pericyte transcriptomic studies where the RFC1 gene was one of the only three consistently detected genes in brain pericytes out of the 1180 enriched genes [44].

Our study provides initial insights regarding the functional importance of RFC1 in retinal microvessels. The genetic knockout of RFC1 is lethal [48] and no conditional knockout animals had been used in the studies before, so we decided to utilize siRNA technology to manipulate RFC1 levels specifically in the retina of adult mice. Two previous in vitro studies using RFC1-siRNA which were performed in primary cultures of human differentiated adipocytes [49], and in rat choroidal epithelial Z310 cells [50], and both did not focus on the microvessels or the retina. Hence, our method to knockdown RFC1 in vivo could be considered as one of the initial studies. RFC1-siRNA administration to the retina in vivo via intravitreal delivery offers some advantages: (1) the retina is the easily reachable, well-known extension of the brain (2) the vitreous cavity is an enclosed space that minimizes the adverse effects of systemic spread and maximizes the effect of applied concentration (3) delivery is fast and feasible [51]. The

(See figure on next page.)

Fig. 4 RFC1 protein increased after retinal ischemia, and the overexpression of RFC1 before ischemia by LV salvaged decreased collagen-4 and occludin levels. **A** The representative Western blotting image from control (n = 5) and ischemic (n = 3) retinas. Housekeeping gene β-Tubulin III was used as loading control. **B** The graph shows the relative density measurements of bands which were calculated by proportioning to loading control. One-hour permanent retinal ischemia increased relative RFC1 protein levels compared to control. **C** Retinal ischemia significantly augmented the percentage of mean grey value of RFC1 by 114.5% (n = 3). Representative confocal images of control or ischemic retinal microvessels stained by anti-RFC1 antibody (red). Significant immunosignal increase in ischemic microvessels was observed compared to controls. Also, ischemic microvessels demonstrated expected characteristics such as constrictions and protruding pericyte bodies (asterisk). Of note, ischemic pericyte bodies showed denser RFC1 immunosignal (white arrows). **D**, **E** In contrast, retinal ischemia decreased collagen-4 by 42.07% (n = 3), occludin by 50.94% (n = 3). **F**, **G** In addition, microvessels treated with LV-RFC1, 10 days before ischemia showed 176% increase in collagen-4 (n = 3) and 60.9% in occludin (n = 3) immunosignal compared to Control-LV delivered ones indicating RFC1 overexpression before ischemia might retrieve loss of collagen-4 and occludin in ischemia. (*$p \leq 0.05$). Nuclei were labelled with Hoechst 33258 (blue) in all images. Data are mean ± S.E.M. Mann-Whitney U; Scale bars= 10 µm

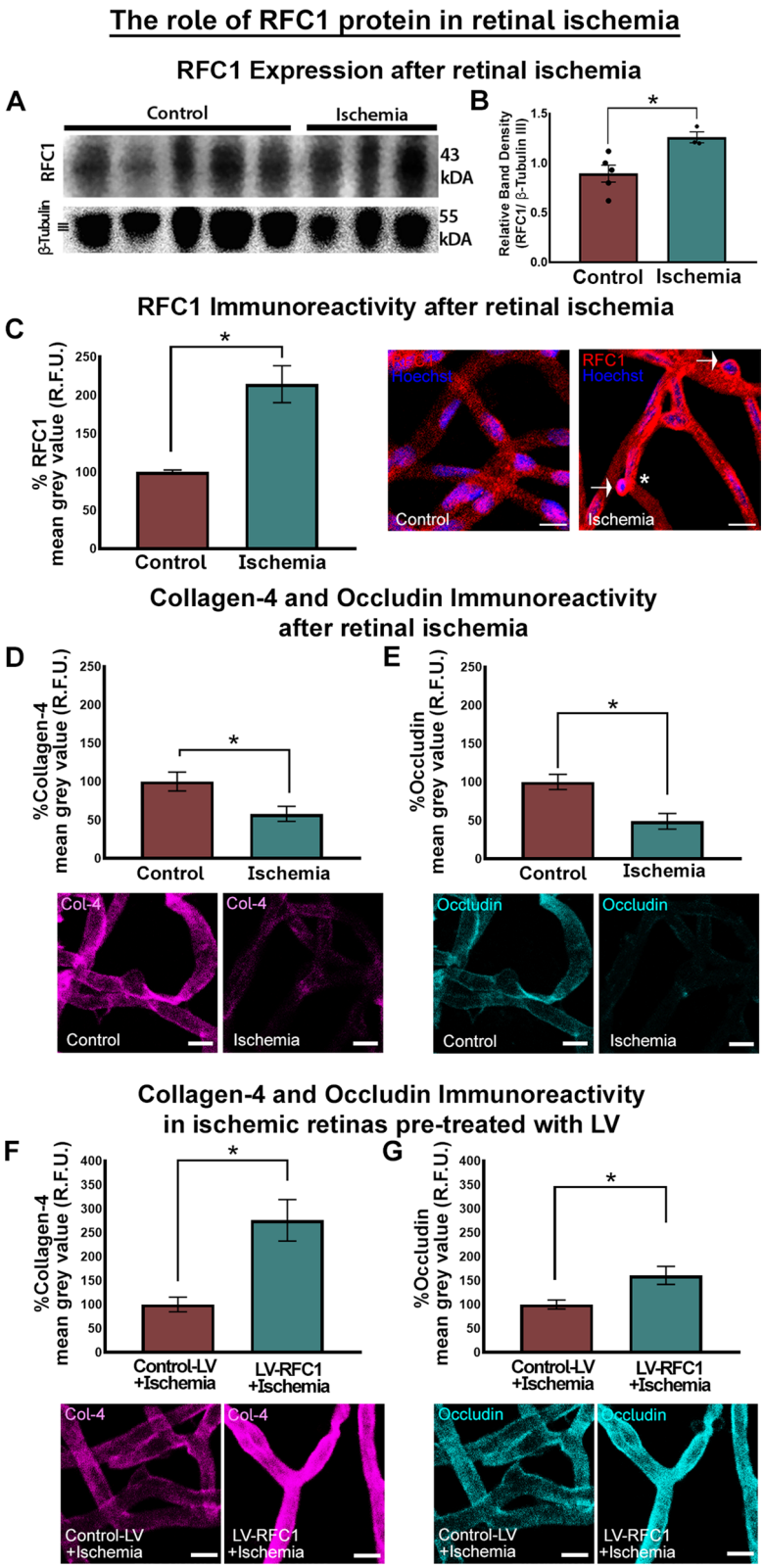

Fig. 4 (See legend on previous page.)

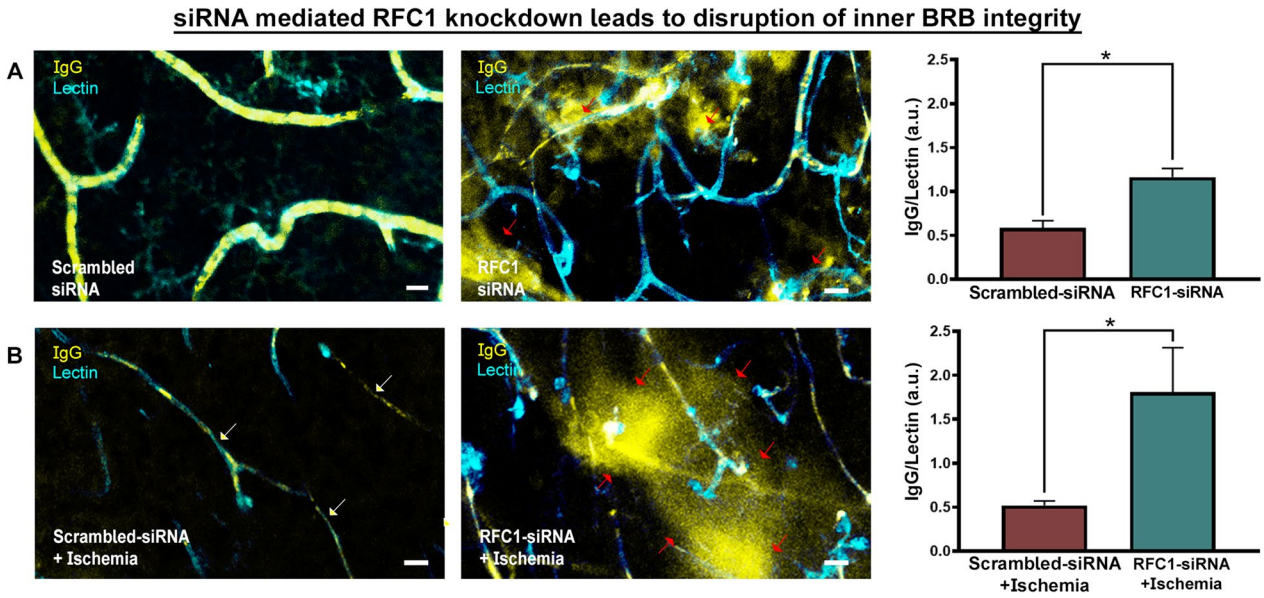

Fig. 5 siRNA mediated RFC1 knockdown led to inner BRB breakdown and endogenous IgG extravasation. The wholemount retinas were labeled by Lectin (cyan) and incubated with Cy3 labeled goat anti-mouse antibody (yellow) to visualize the extravasated endogenous mouse IgG. **A** RFC1-siRNA mediated knockdown led to significant IgG extravasation (red arrows) in microvessels while scrambled-siRNA treated retinas showed no extravascular IgG signal ($p = 0.001$; $n = 3$). **B** 1 h ischemia led to microvessel constrictions (white arrows) but no IgG extravasation. However, knocking down RFC1 before ischemia provoked inner BRB disruption leading to endogenous IgG extravasation (red arrows) ($p = 0.05$; $n = 3$). Nuclei were labelled with Hoechst 33258 (blue) in all images. Scale bars= 10 µm

application of RFC1-siRNA deranged the structure of retinal microvessels, led to a significant decrease in the barrier proteins occludin, claudin-5, ZO-1, and collagen-4, which induced the inner BRB disintegration and functional failure of the barrier. Although it may be plausible to interpret this striking result with caution, there is a study showing that the tight junction proteins like occludin, claudin-1, and ZO-1 were substantially decreased in the BBB of capillaries isolated from proton coupled folate transporter (PCFT) null mice [52]. However, this mouse with deleted PCFT is accepted as a model for hereditary folate malabsorption that leads to systemic folate deficiency. Hence, it is not possible to fully exclude the contribution of chronic folate deficiency to these effects. However, in our study, we observed inner BRB changes after acute modifications of the transporter in naive mice, which circumvents the confounding developmental effects of folate deficiency. Moreover, we confirmed that our RFC1-siRNA treatment did not lead any major structural deterioration despite immersive inner BRB breakdown, which implied the main effect of RFC1 knockdown was primarily observed in the inner BRB. In line with these observations, our experiments with the retinal overexpression of RFC1 via LV have shown an upregulation of occludin, claudin-5 and collagen-4, supporting the role of RFC1 in inner BRB protein expressions. As an interesting observation, RFC1 was recently determined as a cGAMP importer in the cyclic GMP–AMP synthase (cGAS)–stimulator of interferon genes (STING) pathway that has a role in inflammation, cellular stress, and tumor angiogenesis [23, 53, 54]. In mouse tumor models, intratumoral cGAMP treatment led to a decrease in the density of the vessels, a rise in pericyte and collagen-4 coverage [53], which may indicate that RFC1 may be indirectly involved in remodeling the tumor vasculature in consistence with our observations in inner retinal microvasculature.

Based on reports that show pericytes are eminent for BBB and inner BRB maintenance and contribute to tight junction formation and preservation [55–58], we also excluded pericyte deficiency in RFC1-siRNA treated retinas. Although we found no significant decrease in pericyte density and pericyte associated microvascular diameter, we observed immunosignal decrease in pericyte marker NG2 which is involved in many functions of pericytes including proliferation, motility and importantly, endothelial cell junction assembly by activating integrin signaling [59]. For example, the treatment of human microvascular pericytes with NG2-siRNA hindered collagen-4 coverage, ZO-1 expression, and endothelial junction maintenance in endothelial cells. Likewise, tumors from mice whose pericytes do not express NG2 showed similar changes in their endothelial

junctions in the same study [32]. Although the underlying mechanisms require clarification, we suggest that NG2 might be a mediator of the effects observed in tight junction proteins and collagen-4 via RFC1-siRNA. Alternatively, the disintegration of NG2 in RFC1-siRNA treated retinal microvessels may indicate more comprehensive dysfunction throughout the inner BRB, to which NG2 disruption is only a contributing factor.

Aside from its role in the maintenance of inner BRB under physiologic conditions, we further investigated the effect of RFC1 in acute retinal ischemia. Retinal ischemia which is a major underlying condition of blindness worldwide is a severe condition with a poor prognosis generally caused by acute occlusion of retinal arteries. We induced 1 h retinal ischemia by an established method in our laboratory [21, 35], and observed an increase in RFC1 protein. A previous gene profiling study showed RFC1 mRNA upregulation following 1 h ischemia / 24 h recanalization induced by high intraocular pressure retinal ischemia model in rats [60]. In contrast, the same study observed no significant change in RFC1 mRNA in 1 h permanent retinal ischemia. Another study showed that 45 min retinal ischemia followed by 48 h recanalization upregulated RFC1 mRNA in rats [61]. The possible explanation for these results may be that the retinal ischemia models were different, and the authors only determined mRNA levels, not the protein levels of the samples. The estimation of protein levels from mRNA levels might be unreliable, as post-translational changes could affect the protein levels in early time-points [62]. There is only one study performed by kidney ischemia–reperfusion model that determined RFC1 protein levels decreased in vivo focusing on the proximal tubules where folate reabsorption occurs, emphasizing its importance in adjusting serum folate levels [63]. Several candidate mechanisms offer clues to RFC1 regulation in ischemia, which should be considered only as suggestive with inconclusive evidence for the time being. (1) It has been shown that nitric oxide (NO) has a direct impact on the expression and function of RFC1 by modifying the thiol groups in the protein resulting in decrease in the activity of RFC1. Production of NO in ischemic-hypoxic state leading to decrease in substrate affinity of active form of folate may result in RFC1 protein level upregulation since the regulation of RFC1 is closely linked to folate balance in vivo. For instance, in vitro studies of cell lines showed that prolonged culture with reduced folate concentrations below normal levels resulted in increased levels of RFC1 [64–66]. Furthermore, in mice that were fed with folate-deficient diets, there was an increase in RFC transcripts and proteins in the small intestine [67]. In short, ischemia-induced NO production could lead to activity inhibition of RFC1, ultimately resulting in the upregulation of its protein levels. (2) RFC1 has been defined as one of the 198 hypoxia-related genes in the Molecular Signatures Database [24] (MSigDB, https://www.gsea-msigdb.org/gsea/msigdb/). In one study, isolated mouse skin endothelial cells exposed to hypoxia had an upregulation in RFC1 in the absence of HIF-1α. However, in another study, cultured endothelial cells from human pulmonary arteries exposed to hypoxia had downregulation of RFC1 mRNA expression [68]. Both studies together suggest HIF-1α is required for downregulating RFC1 in hypoxia. However, we should regard that both studies were done in cultured cells that had been passaged for more than one time. The literature also suggests that RFC1 is upregulated in cultured cells to meet the folate need of proliferating cells [69]. Thus, cultured cells used in these studies must have already expressed more than enough RFC1 than naive, in vivo state of endothelial cells. This could change the regulation of the RFC1 gene in the ischemic state aside from the changes brought by removing cells from their in vivo niche. (3) A recent study has identified Nuclear respiratory factor 1 (NRF-1) as the regulator of RFC1 at the blood–brain barrier [70]. Additionally, NRF-1 transcriptionally regulates HIF-1α by acting as the repressor of the gene. The upregulation of NRF-1 in ganglion cell layers and inner nuclear cell layers in ischemic rats coincided with the layers nourished by inner BRB. Overall, NRF-1 may play a complex role in regulating RFC1 in ischemia. Alternatively, the increase of metabolic needs due to acute phase of ischemia might necessitate the upregulation of RFC1 after 1 h of retinal ischemia for the preservation of the barrier properties. In line with that, further augmentation of RFC1 expression by LV-RFC1 intervention before ischemia salvaged the decreased occludin and collagen-4 levels, otherwise which would be attenuated by ischemia.

Also, knocking down RFC1 prior to ischemia impaired barrier functions which were demonstrated by endogenous IgG leakage, supporting our findings that RFC1 is essential for the protection of inner BRB during retinal ischemia. This result might be interpreted in the light of the human meta-analysis showing that the SNPs of RFC1 gene differed between ischemic stroke and control groups, and some genotypes were found to be associated with small vessel occlusions and silent brain infarctions [71]. Since the changes in RFC1 function or structure with these polymorphisms had not been defined, it is possible that our finding of changes in inner BRB via the genetic modifications of RFC1 could carry the potential of being the experimental evidence of the importance of RFC1 in ischemia and small vessel disease. Thus, intriguing questions regarding the therapeutic potential of intervening RFC1 before, during or after ischemia rises.

Our study is an initial step to investigate the role of 'once an unnoticed transporter protein' in the inner BRB. We took a step-by-step approach, defined the presence of the RFC1 protein in the retinal microvessels and established in vivo genetic tools to clarify the potential new roles of RFC1 under physiologic conditions, ischemia. However, some limitations of our study merit consideration. The genetic manipulations we used were not targeted to cells. In addition, we did not study the underlying pathways of how RFC1 regulates barrier proteins or BRB integrity, and the interplay of folate and other folate transport systems (FRα and PCFT) or the concert of the efflux systems (Pgp/ABCB1, MRPs/ABCC, BCRP/ABCG2) [72], which warrants further investigations.

Despite these limitations, our data suggest several implications. We propose a conceptual model of workflow for the other proteins like RFC1 whose presence and roles have not been elucidated so far. Nowadays, the roles of these proteins have been investigated through advanced mathematical models, pathway analyses and the -omics approaches, but the old phrase "seeing is believing" should not be underestimated and in vivo studies may provide surprising insights into the role of a protein. The upregulation of RFC1 may be attempted for diseases other than ischemia where the impairment of BRB or BBB is involved in the pathophysiology. Although merely an initial step, our results are encouraging as the presence of RFC1 in inner BRB may be exploited for targeted drug delivery such as RFC1-targeted nanodrugs, folate conjugated nanodrugs or even clinically widely used RFC1 substrate, methotrexate, can be exploited not only in cancer, but in diseases like ischemia.

Conclusion

In the present study, we investigated the presence of RFC1 in the retinal endothelial cells and pericytes, and its role in the regulation of inner BRB integrity. For the first time, we introduced and discussed the tools for the manipulation of RFC1 levels or function in vivo which included RFC1-targeted Accell siRNA to knockdown RFC1, and LV to overexpress RFC1. By using these tools, we tried to elucidate the role of RFC1 in the abrupt regulation of inner BRB during physiological conditions and acute retinal ischemia and highlighted its potential role for preserving BRB integrity. This study aimed to precede the further investigation of RFC1 in other tissues and diseases by suggesting a conceptual and methodological framework. Future research may extend this work by integrating pathways which RFC1 is associated with to address the concern of how RFC1 regulates inner BRB.

Abbreviations

BBB	Blood–brain barrier
BRB	Blood-retina barrier
CD13	Aminopeptidase N
cGAMP	Cyclic guanosine monophosphate–adenosine
cGAS	Cyclic GMP-AMP synthase
GCL	Ganglion cell layer
HIF-1α	Hypoxia-inducible factor 1-alpha
IgG	Immunoglobulin G
INL	Inner nuclear layer
IPL	Inner plexiform layer
LSCI	Laser speckle contrast imaging
LV	Lentiviral vectors
mRNA	Messenger RNA
MTX	Methotrexate
NG2	Neural/glial antigen 2
NRF-1	Nuclear respiratory factor 1
ONL	Outer nuclear layer
OPL	Outer plexiform layer
PBS	Phosphate buffered saline
PDGFR-β	Platelet-derived growth factor receptor beta
PFA	Paraformaldehyde
qRT-PCR	Quantitative reverse transcriptase-polymerase chain reaction
RFC1	Reduced Folate Carrier 1
RIPA	Radio immune precipitation assay
RPE	Retinal pigmented epithelium
siRNA	Short interfering RNA
SLC19a1	Solute carrier family 19 (folate transporter), member 1
SNPs	Single nucleotide polymorphisms
STING	Stimulator of interferon genes
UV	Ultraviolet
ZO-1	Zonula occludens 1

Supplementary Information

The online version contains supplementary material available at https://doi.org/10.1186/s12987-023-00442-3.

Additional file 1: Fig. S1. Super-resolution microscopy of retinal radial sections to reveal the distribution of RFC1 protein over the endothelial cell surface. (A) 3D reconstruction of RFC1 immunostaining performed by MyBioSource antibody which is targeted to N-terminal region of protein. (B) 3D reconstruction of RFC1 immunostaining performed by Sigma antibody which is targeted to C-terminal region of the protein. In both stainings, RFC1 puncta are localized to the luminal endothelial cell surface stained by CD31 (white arrows). RFC1 puncta are also visible from the abluminal side (yellow arrows), indicating abluminal endothelial membrane or pericyte localization of RFC1 protein. Scale bars=10 µm.

Additional file 2: Fig S2. Effects of siRNA mediated RFC1 knockdown in the retina. A Representative scotopic (dark-adapted) electroretinogram (ERG). The ERG recordings include measurements of the a-wave, b-wave, and implicit time of a-wave peak and b-wave peak. The amplitude of the a-wave is determined by measuring the distance between the baseline and the lowest point of the negative deflection. On the other hand, the amplitude of the b-wave is calculated by measuring the distance between the maximum point of the a-wave and the peak of the positive deflection of the b-wave. 0 mV indicates baseline response. B, C Comparison of mean amplitudes ± SEM of scotopic a-wave and b-wave between Scrambled-siRNA and RFC1-siRNA treated mice. D, E Comparison of mean implicit time ± SEM of A-wave peak and B-wave peak between scrambled-siRNA and RFC1-siRNA mice. Only average of the implicit time B-wave peak between Scrambled-siRNA (55±3.0 ms) and RFC1-siRNA (71±2.7 ms) was different (p=0.029; n=4/group). F β-Tubulin III (red), Lectin (green), and Hoechst 33258 (blue) stained central retinal cross-sections were imaged with confocal microscopy. To manually count GC number, ROIs in 250 µm length were placed on the ganglion cell layer. Total retinal thickness was determined from the nerve fiber layer to retinal pigment epithelium. The width of the INL (the distance between the inner plexiform layer and the outer plexiform layer) and ONL (the distance between the outer plexiform

layer and the outer limiting membrane) were determined by a fluorescent nuclear dye (Hoechst 33258). G-J The bar graphs show that there is no statistically significant difference in the abovementioned parameters between RFC1-siRNA and Scrambled-siRNA treated groups (n=3/per group). *p=0.029, data are mean ± S.E.M Mann-Whitney U; Scale bar: 25 µm. GC: ganglion cell, INL: inner nuclear layer, ONL: outer nuclear layer, ROI: Region of interest.

Acknowledgements
We thank Dr. Canan Cakir Aktas (The Institute of Neurological Sciences and Psychiatry, Hacettepe University, Ankara, Turkey) for assisting the financial management of the project, Dr. Buket Nebiye Demir (The Institute of Neurological Sciences and Psychiatry, Hacettepe University, Ankara, Turkey) for technical advice on in vivo procedures, Dr. Cetin Demir (Faculty of Medicine, Department of Pediatrics, Division of Pediatric Oncology, Drug Resistance Laboratory, Hacettepe University, Ankara, Turkey) for his assistance in the execution of qRT-PCR experiments, Dr. Umit Can Erim (Faculty of Pharmacy, Istanbul Medipol University, Istanbul, Turkey) for his meticulous work for folate measurement requested in the revision, and our laboratory technician Mesut Firat (The Institute of Neurological Sciences and Psychiatry, Hacettepe University, Ankara, Turkey) for providing technical assistance throughout project. We are grateful to our undergraduate researchers Derin Nalcakan and Neslihan Nisa Gecici (Hacettepe University Medical School), who were officially added as interns to the project with "TÜBİTAK-Intern Researcher Scholarship Programme", for their contribution to immunohistochemistry and data analysis.

Author contributions
GG contributed to the study design, performed surgeries and experiments, obtained tissues, performed immunohistochemistry, collected images and data, analyzed the data, prepared figures, wrote the draft of the manuscript and contributed to editing. NB contributed to the design and execution of Western Blottings and collected membrane images. MCB designed and synthesized the lentiviral vector and performed cell-line Western Blottings. MSB contributed to the design and execution of qRT-PCR experiments and performed related analysis. GU contributed to the in vivo application of retinal ischemia model, retinal trypsin digestion and intravitreal injections, and writing of the paper. UCE developed folate measurement method required in the revision, contributed to the manuscript. EK provided lentiviral vector as a courtesy and contributed to editing. MY acquired funds and administered the project, coordinated, and supervised the work, wrote the manuscript, and contributed to figures and edited the paper. All authors read and approved the final manuscript.

Funding
This research was supported by The Scientific and Technological Research Institution of Turkey (TÜBİTAK; Grant No: 120N690) to MY and Hacettepe University Scientific Research Projects Coordination Unit (Project No: TDK-2020–18590) to MY.

Availability of data and materials
All data generated or analyzed during this study are included in this published article. Raw data and analyses can be provided upon request. There are no restrictions on data availability.

Declarations

Competing interests
The authors declare that they have no competing interests.

Author details
[1]The Institute of Neurological Sciences and Psychiatry, Hacettepe University, Ankara, Turkey. [2]Biotechnology Institute, Ankara University, Ankara, Turkey. [3]Physiology, Istanbul Medipol University, Istanbul, Turkey. [4]Faculty of Medicine, Department of Neurology, Hacettepe University, Ankara, Turkey. [5]Neuroscience and Neurotechnology Center of Excellence (NÖROM), Ankara, Turkey. [6]Physiology, Istanbul Medeniyet University, Istanbul, Turkey.

Received: 24 December 2022 Accepted: 18 May 2023
Published online: 16 June 2023

References

1. Alam C, Hoque MT, Finnell RH, Goldman ID, Bendayan R. Regulation of reduced folate carrier (RFC) by vitamin D receptor at the blood-brain barrier. Mol Pharmaceut. 2017;14(11):3848–58.
2. Alam C, Aufreiter S, Georgiou CJ, Hoque MT, Finnell RH, O'Connor DL, et al. Upregulation of reduced folate carrier by vitamin D enhances brain folate uptake in mice lacking folate receptor alpha. Proc Natl Acad Sci U S A. 2019;116(35):17531–40.
3. Figueiredo JC, Levine AJ, Grau MV, Midttun O, Ueland PM, Ahnen DJ, et al. Vitamins B2, B6, and B12 and risk of new colorectal adenomas in a randomized trial of aspirin use and folic acid supplementation. Cancer Epidemiol Biomarkers Prev. 2008;17(8):2136–45.
4. Balashova OA, Visina O, Borodinsky LN. Folate action in nervous system development and disease. Dev Neurobiol. 2018;78(4):391–402.
5. Desai A, Sequeira JM, Quadros EV. The metabolic basis for developmental disorders due to defective folate transport. Biochimie. 2016;126:31–42.
6. Mentch SJ, Locasale JW. One-carbon metabolism and epigenetics: understanding the specificity. Ann N Y Acad Sci. 2016;1363:91–8.
7. Lehmann M, Regland B, Blennow K, Gottfries CG. Vitamin B12-B6-folate treatment improves blood-brain barrier function in patients with hyperhomocysteinaemia and mild cognitive impairment. Dement Geriatr Cogn Disord. 2003;16(3):145–50.
8. Snowdon DA, Tully CL, Smith CD, Riley KP, Markesbery WR. Serum folate and the severity of atrophy of the neocortex in Alzheimer disease: findings from the Nun study. Am J Clin Nutr. 2000;71(4):993–8.
9. Sofi F, Marcucci R, Bolli P, Giambene B, Sodi A, Fedi S, et al. Low vitamin B6 and folic acid levels are associated with retinal vein occlusion independently of homocysteine levels. Atherosclerosis. 2008;198(1):223–7.
10. Cahill MT, Stinnett SS, Fekrat S. Meta-analysis of plasma homocysteine, serum folate, serum vitamin B(12), and thermolabile MTHFR genotype as risk factors for retinal vascular occlusive disease. Am J Ophthalmol. 2003;136(6):1136–50.
11. Rajamani R, Muthuvel A, Senthilvelan M, Sheeladevi R. Oxidative stress induced by methotrexate alone and in the presence of methanol in discrete regions of the rodent brain, retina and optic nerve. Toxicol Lett. 2006;165(3):265–73.
12. Schneider MP, Schlaich MP, Harazny JM, Raff U, Ritt M, Ott C, et al. Folic acid treatment normalizes NOS-dependence of vascular tone in the metabolic syndrome. Obesity. 2011;19(5):960–7.
13. Kaur C, Foulds WS, Ling EA. Blood-retinal barrier in hypoxic ischaemic conditions: basic concepts, clinical features and management. Prog Retin Eye Res. 2008;27(6):622–47.
14. London A, Benhar I, Schwartz M. The retina as a window to the brain-from eye research to CNS disorders. Nat Rev Neurol. 2013;9(1):44–53.
15. Cunha-Vaz J, Bernardes R, Lobo C. Blood-retinal barrier. Eur J Ophthalmol. 2011;21(Suppl 6):S3-9.
16. Naggar H, Ola MS, Moore P, Huang W, Bridges CC, Ganapathy V, et al. Downregulation of reduced-folate transporter by glucose in cultured RPE cells and in RPE of diabetic mice. Invest Ophthalmol Vis Sci. 2002;43(2):556–63.
17. Naggar H, Fei YJ, Ganapathy V, Smith SB. Regulation of reduced-folate transporter-1 (RFT-1) by homocysteine and identity of transport systems for homocysteine uptake in retinal pigment epithelial (RPE) cells. Exp Eye Res. 2003;77(6):687–97.
18. Bridges CC, El-Sherbeny A, Ola MS, Ganapathy V, Smith SB. Transcellular transfer of folate across the retinal pigment epithelium. Curr Eye Res. 2002;24(2):129–38.
19. Smith SB, Huang W, Chancy C, Ganapathy V. Regulation of the reduced-folate transporter by nitric oxide in cultured human retinal pigment epithelial cells. Biochem Biophys Res Commun. 1999;257(2):279–83.
20. Yemisci M, Gursoy-Ozdemir Y, Vural A, Can A, Topalkara K, Dalkara T. Pericyte contraction induced by oxidative-nitrative stress impairs capillary reflow despite successful opening of an occluded cerebral artery. Nat Med. 2009;15(9):1031-U82.

21. Alarcon-Martinez L, Yilmaz-Ozcan S, Yemisci M, Schallek J, Kilic K, Villafranca-Baughman D, et al. Retinal ischemia induces alpha-SMA-mediated capillary pericyte contraction coincident with perivascular glycogen depletion. Acta Neuropathol Commun. 2019;7(1):134.
22. Alarcon-Martinez L, Yilmaz-Ozcan S, Yemisci M, Schallek J, Kilic K, Can A, et al. Capillary pericytes express alpha-smooth muscle actin, which requires prevention of filamentous-actin depolymerization for detection. Elife. 2018. https://doi.org/10.7554/eLife.34861.
23. Ritchie C, Cordova AF, Hess GT, Bassik MC, Li L. SLC19A1 Is an importer of the immunotransmitter cGAMP. Mol Cell. 2019;75(2):372–81.
24. Li W, Yuan P, Liu W, Xiao L, Xu C, Mo Q, et al. Hypoxia-immune-related gene SLC19A1 serves as a potential biomarker for prognosis in multiple myeloma. Front Immunol. 2022;13: 843369.
25. Chou JC, Rollins SD, Fawzi AA. Trypsin digest protocol to analyze the retinal vasculature of a mouse model. J Vis Exp. 2013;76: e50489.
26. Zudaire E, Gambardella L, Kurcz C, Vermeren S. A computational tool for quantitative analysis of vascular networks. PLoS ONE. 2011;6(11): e27385.
27. Feng D, Nagy JA, Pyne K, Dvorak HF, Dvorak AM. Ultrastructural localization of platelet endothelial cell adhesion molecule (PECAM-1, CD31) in vascular endothelium. J Histochem Cytochem. 2004;52(1):87–101.
28. Kureli G, Yilmaz-Ozcan S, Erdener SE, Donmez-Demir B, Yemisci M, Karatas H, et al. F-actin polymerization contributes to pericyte contractility in retinal capillaries. Exp Neurol. 2020;332: 113392.
29. Discovery H. Accell™ siRNA References 8100 Cambridge Research Park, Waterbeach, Cambridge, CB25 9TL, United Kingdom2021 [Available from: https://horizondiscovery.com/-/media/Files/Horizon/resources/Reading-lists/accell-sirna-ref-reading.pdf.
30. Taniguchi T, Endo KI, Tanioka H, Sasaoka M, Tashiro K, Kinoshita S, et al. Novel use of a chemically modified siRNA for robust and sustainable in vivo gene silencing in the retina. Sci Rep. 2020;10(1):22343.
31. Calkins DJ, Yu-Wai-Man P, Newman NJ, Taiel M, Singh P, Chalmey C, et al. Biodistribution of intravitreal (lenadogene) nolparvovec gene therapy in nonhuman primates. Mol Ther Methods Clin Dev. 2021;23:307–18.
32. You WK, Yotsumoto F, Sakimura K, Adams RH, Stallcup WB. NG2 proteoglycan promotes tumor vascularization via integrin-dependent effects on pericyte function. Angiogenesis. 2014;17(1):61–76.
33. Beker M, Caglayan AB, Beker MC, Altunay S, Karacay R, Dalay A, et al. Lentivirally administered glial cell line-derived neurotrophic factor promotes post-ischemic neurological recovery, brain remodeling and contralesional pyramidal tract plasticity by regulating axonal growth inhibitors and guidance proteins. Exp Neurol. 2020;331: 113364.
34. Brandli A, Stone J. Using the electroretinogram to assess function in the rodent retina and the protective effects of remote limb ischemic preconditioning. J Vis Exp. 2015;100: e52658.
35. Karatas H, Erdener SE, Gursoy-Ozdemir Y, Gurer G, Soylemezoglu F, Dunn AK, et al. Thrombotic distal middle cerebral artery occlusion produced by topical FeCl(3) application: a novel model suitable for intravital microscopy and thrombolysis studies. J Cereb Blood Flow Metab. 2011;31(6):1452–60.
36. Hinken M, Halwachs S, Kneuer C, Honscha W. Subcellular localization and distribution of the reduced folate carrier in normal rat tissues. Eur J Histochem. 2011;55(1): e3.
37. Trippett TM, Garcia S, Manova K, Mody R, Cohen-Gould L, Flintoff W, et al. Localization of a human reduced folate carrier protein in the mitochondrial as well as the cell membrane of leukemia cells. Cancer Res. 2001;61(5):1941–7.
38. Chancy CD, Kekuda R, Huang W, Prasad PD, Kuhnel JM, Sirotnak FM, et al. Expression and differential polarization of the reduced-folate transporter-1 and the folate receptor alpha in mammalian retinal pigment epithelium. J Biol Chem. 2000;275(27):20676–84.
39. Wei Y, Gong J, Xu Z, Thimmulappa RK, Mitchell KL, Welsbie DS, et al. Nrf2 in ischemic neurons promotes retinal vascular regeneration through regulation of semaphorin 6A. Proc Natl Acad Sci U S A. 2015;112(50):E6927-36.
40. Auricchio A, Kobinger G, Anand V, Hildinger M, O'Connor E, Maguire AM, et al. Exchange of surface proteins impacts on viral vector cellular specificity and transduction characteristics: the retina as a model. Hum Mol Genet. 2001;10(26):3075–81.
41. Wang X, Liu Y, Sun Y, Liu W, Jin X. Blood brain barrier breakdown was found in non-infarcted area after 2-h MCAO. J Neurol Sci. 2016;363:63–8.
42. Chen B, Friedman B, Cheng Q, Tsai P, Schim E, Kleinfeld D, et al. Severe blood-brain barrier disruption and surrounding tissue injury. Stroke. 2009;40(12):e666-74.
43. Jin X, Liu J, Yang Y, Liu KJ, Yang Y, Liu W. Spatiotemporal evolution of blood brain barrier damage and tissue infarction within the first 3h after ischemia onset. Neurobiol Dis. 2012;48(3):309–16.
44. He L, Vanlandewijck M, Raschperger E, Andaloussi Mae M, Jung B, Lebouvier T, et al. Analysis of the brain mural cell transcriptome. Sci Rep. 2016;6:35108.
45. Hosoya K, Fujita K, Tachikawa M. Involvement of reduced folate carrier 1 in the inner blood-retinal barrier transport of methyltetrahydrofolate. Drug Metab Pharmacokinet. 2008;23(4):285–92.
46. Sangha V, Hoque MT, Henderson JT, Bendayan R. Novel localization of folate transport systems in the murine central nervous system. Fluids Barriers CNS. 2022;19(1):92.
47. Geier EG, Chen EC, Webb A, Papp AC, Yee SW, Sadee W, et al. Profiling solute carrier transporters in the human blood-brain barrier. Clin Pharmacol Ther. 2013;94(6):636–9.
48. Zhao R, Russell RG, Wang Y, Liu L, Gao F, Kneitz B, et al. Rescue of embryonic lethality in reduced folate carrier-deficient mice by maternal folic acid supplementation reveals early neonatal failure of hematopoietic organs. J Biol Chem. 2001;276(13):10224–8.
49. Petrus P, Bialesova L, Checa A, Kerr A, Naz S, Backdahl J, et al. Adipocyte expression of SLC19A1 links DNA hypermethylation to adipose tissue inflammation and insulin resistance. J Clin Endocrinol Metab. 2018;103(2):710–21.
50. Grapp M, Wrede A, Schweizer M, Huwel S, Galla HJ, Snaidero N, et al. Choroid plexus transcytosis and exosome shuttling deliver folate into brain parenchyma. Nat Commun. 2013;4:2123.
51. Meyer CH, Krohne TU, Charbel Issa P, Liu Z, Holz FG. Routes for drug delivery to the eye and retina: intravitreal injections. Dev Ophthalmol. 2016;55:63–70.
52. Wang X, Cabrera RM, Li Y, Miller DS, Finnell RH. Functional regulation of P-glycoprotein at the blood-brain barrier in proton-coupled folate transporter (PCFT) mutant mice. FASEB J. 2013;27(3):1167–75.
53. Yang H, Lee WS, Kong SJ, Kim CG, Kim JH, Chang SK, et al. STING activation reprograms tumor vasculatures and synergizes with VEGFR2 blockade. J Clin Invest. 2019;129(10):4350–64.
54. Luteijn RD, Zaver SA, Gowen BG, Wyman SK, Garelis NE, Onia L, et al. SLC19A1 transports immunoreactive cyclic dinucleotides. Nature. 2019;573(7774):434–8.
55. Al Ahmad A, Gassmann M, Ogunshola OO. Maintaining blood-brain barrier integrity: pericytes perform better than astrocytes during prolonged oxygen deprivation. J Cell Physiol. 2009;218(3):612–22.
56. Yang T, Guo L, Fang Y, Liang M, Zheng Y, Pan M, et al. Pericytes of indirect contact coculture decrease integrity of inner blood-retina barrier model in vitro by upgrading MMP-2/9 activity. Dis Markers. 2021;2021:7124835.
57. Daneman R, Zhou L, Kebede AA, Barres BA. Pericytes are required for blood-brain barrier integrity during embryogenesis. Nature. 2010;468(7323):562–6.
58. Bell RD, Winkler EA, Sagare AP, Singh I, LaRue B, Deane R, et al. Pericytes control key neurovascular functions and neuronal phenotype in the adult brain and during brain aging. Neuron. 2010;68(3):409–27.
59. Stallcup WB. The NG2 proteoglycan in pericyte biology. Adv Exp Med Biol. 2018;1109:5–19.
60. Andreeva K, Zhang M, Fan W, Li X, Chen Y, Rebolledo-Mendez JD, et al. Time-dependent gene profiling indicates the presence of different phases for ischemia/reperfusion injury in retina. Ophthalmol Eye Dis. 2014;6:43–54.
61. Abcouwer SF, Lin CM, Wolpert EB, Shanmugam S, Schaefer EW, Freeman WM, et al. Effects of ischemic preconditioning and bevacizumab on apoptosis and vascular permeability following retinal ischemia-reperfusion injury. Invest Ophthalmol Vis Sci. 2010;51(11):5920–33.
62. Fortelny N, Overall CM, Pavlidis P, Freue GVC. Can we predict protein from mRNA levels? Nature. 2017;547(7664):E19–20.
63. Yang C, Wijerathne CUB, Tu GW, Woo CWH, Siow YL, Madduma Hewage S, et al. Ischemia-reperfusion injury reduces kidney folate transporter expression and plasma folate levels. Front Immunol. 2021;12: 678914.
64. Sirotnak FM, Moccio DM, Yang CH. A novel class of genetic variants of the L1210 cell up-regulated for folate analogue transport inward. Isolation,

characterization, and degree of metabolic instability of the system. J Biol Chem. 1984;259(21):13139–44.
65. Matherly LH, Czajkowski CA, Angeles SM. Identification of a highly glycosylated methotrexate membrane carrier in K562 human erythroleukemia cells up-regulated for tetrahydrofolate cofactor and methotrexate transport. Cancer Res. 1991;51(13):3420–6.
66. Jansen G, Westerhof GR, Jarmuszewski MJ, Kathmann I, Rijksen G, Schornagel JH. Methotrexate transport in variant human CCRF-CEM leukemia cells with elevated levels of the reduced folate carrier selective effect on carrier-mediated transport of physiological concentrations of reduced folates. J Biol Chem. 1990;265(30):18272–7.
67. Liu M, Ge Y, Cabelof DC, Aboukameel A, Heydari AR, Mohammad R, et al. Structure and regulation of the murine reduced folate carrier gene: identification of four noncoding exons and promoters and regulation by dietary folates. J Biol Chem. 2005;280(7):5588–97.
68. Manalo DJ, Rowan A, Lavoie T, Natarajan L, Kelly BD, Ye SQ, et al. Transcriptional regulation of vascular endothelial cell responses to hypoxia by HIF-1. Blood. 2005;105(2):659–69.
69. Bozard BR, Ganapathy PS, Duplantier J, Mysona B, Ha Y, Roon P, et al. Molecular and biochemical characterization of folate transport proteins in retinal muller cells. Invest Ophthalmol Vis Sci. 2010;51(6):3226–35.
70. Alam C, Hoque MT, Sangha V, Bendayan R. Nuclear respiratory factor 1 (NRF-1) upregulates the expression and function of reduced folate carrier (RFC) at the blood-brain barrier. FASEB J. 2020;34(8):10516–30.
71. Cho Y, Kim JO, Lee JH, Park HM, Jeon YJ, Oh SH, et al. Association of reduced folate carrier-1 (RFC-1) polymorphisms with ischemic stroke and silent brain infarction. PLoS ONE. 2015;10(2): e0115295.
72. Assaraf YG. The role of multidrug resistance efflux transporters in antifolate resistance and folate homeostasis. Drug Resist Updat. 2006;9(4–5):227–46.

Publisher's Note